STRUCTURAL SCIENCE CRYSTAL ENGINEERING MATERIALS

ISSN 2052-5206

At last! The single-crystal X-ray structure of a naturally occurring sample of the ilmenite-type oxide $FeCrO_3$

María Ana Pérez-Cruz,[a] María de la Paz Elizalde-González,[b] Roberto Escudero,[c] Sylvain Bernès,[d]* Rutilo Silva-González[d] and Yasmi Reyes-Ortega[b]

[a]Facultad de Ciencias Químicas, Benemérita Universidad Autónoma de Puebla, Edif. 105I Complejo de Ciencias CU, San Manuel, 72570 Puebla, Pue., Mexico, [b]Centro de Química del Instituto de Ciencias, Benemérita Universidad Autónoma de Puebla, Edif. F103 Complejo de Ciencias CU, San Manuel, 72570 Puebla, Pue., Mexico, [c]Instituto de Investigaciones en Materiales, UNAM, Circuito Exterior, Ciudad Universitaria, Coyoacán, 04510 México D.F., Mexico, and [d]Instituto de Física, Benemérita Universidad Autónoma de Puebla, Av. San Claudio y 18 Sur, 72570 Puebla, Pue., Mexico.
*Correspondence e-mail: sylvain_bernes@hotmail.com

Received 8 April 2015
Accepted 24 August 2015

Edited by N. B. Bolotina, Russian Academy of Sciences, Russia

Keywords: mineral; double oxide; ilmenite; magnetism.

CCDC reference: 1420333

Supporting information: this article has supporting information at journals.iucr.org/b

A natural single crystal of the ferrimagnetic oxide $FeCrO_3$, which was found in an opencast mine situated in the San Luis Potosí State in Mexico, has been characterized in order to elucidate some outstanding issues about the actual structure of this material. The single-crystal X-ray analysis unambiguously shows that transition metal cations are segregated in alternating layers normal to the threefold crystallographic axis, affording a structure isomorphous to that of ilmenite ($FeTiO_3$), in the space group $R\overline{3}$. The possible occurrence of cation antisite and vacancy defects is below the limit of detection available from X-ray data. Structural and magnetic results are in agreement with the coherent slow intergrowth of magnetic phases provided by the two antiferromagnetic corundum-type parent oxides Fe_2O_3 (hematite) and Cr_2O_3 (eskolaite). Our results are consistent with the most recent density functional theory (DFT) studies carried out on digital $FeCrO_3$ [Sadat Nabi & Pentcheva (2011). *Phys. Rev. B*, **83**, 214424], and suggest that synthetic samples of $FeCrO_3$ might present a cation distribution different to that of the ilmenite structural type.

1. Introduction and chemical context

Phase diagrams, and the structural and spectroscopic data of iron and chromium oxide solid solutions with corundum or spinel structures have been studied due to their interesting structural and magnetic properties. Some applications are related to heterogeneous catalysis of the dehydrogenation of ethylbenzenes, oxidative dehydrogenation of butenes, selective catalytic reduction of NO_x to ammonia, combustion catalysts, pigments, sensor technologies and data storage based on CrO_2 materials, among others. The phase diagram of the binary system of corundum-type sesquioxides α-Cr_2O_3 (eskolaite) and α-Fe_2O_3 (hematite) shows the existence of a stable, non-Vegardian, continuous solid solution α-$Fe_{2-x}Cr_xO_3$ ($0 < x < 2$), which retains the corundum structure at high temperatures. Metastability and two-phase regions have been described below 1173 K (Musić *et al.*, 1993; Murakami *et al.*, 1999). However, single-phase materials can be restored after annealing above 873 K for at least 1000 h (Murakami *et al.*, 2003).

These mixed oxides may be readily obtained by ceramic procedures (Musić *et al.*, 1996; Loudghiri *et al.*, 2000; Ozkendir, 2013) or by co-precipitation of relevant nitrates or hydroxides, affording fine crystalline powders (Busca *et al.*,

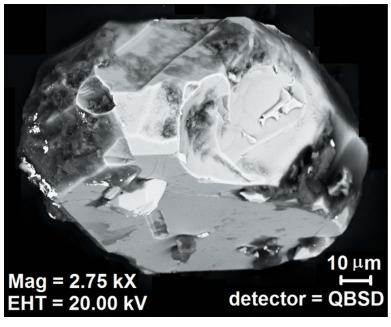

1993; Tsokov *et al.*, 1993; Baraton *et al.*, 1994), microparticles (Grygar, 1999), amorphous (Murakami *et al.*, 1999) or nanocrystalline materials (Bhattacharya *et al.*, 1997). More recently, alternative routes have been explored such as direct alloying assisted by a thermal annealing process (Baca Arroyo *et al.*, 2012) and heteroepitaxial growth of an α-Cr_2O_3 layer onto an α-Fe_2O_3 nanorod array (Vayssieres *et al.*, 2001). Mössbauer (Klinger *et al.*, 1995; Musić *et al.*, 1996; Bhattacharya *et al.*, 1997; Loudghiri *et al.*, 2000; Grygar *et al.*, 2003), XANES (Schmuki, 1998; Ozkendir, 2013) and electronic spectra (Busca *et al.*, 1993; Lenglet *et al.*, 1995; Grygar *et al.*, 2003) have confirmed that oxidation states of metals are Fe^{3+} and Cr^{3+}. Of special interest is the $x = 1$ inter-oxide composition $FeCrO_3$, since the two-phase coexistence region was shown to be metastable at that composition (Grygar *et al.*, 2003), while the equilibrium state of $FeCrO_3$ in the 873–1173 K range was found to be a single phase of the corundum-type solid solution (Murakami *et al.*, 2003). Importantly, some authors suggest that apparent immiscibility is only kinetically conditioned, because end oxides present faster kinetics of crystallization than solid solution members around the $x = 1$ composition (Grygar *et al.*, 2003).

Various cation distributions are consistent with the corundum structural type. In the parent sesquioxides, Cr_2O_3 and Fe_2O_3, the hexagonal close-packed array of O^{2-} ions provides octahedral sites, two-third of which being occupied by cations, and the resulting space group is then $R\overline{3}c$, at least until magnetic ordering is considered (for a very recent reassessment of α-Cr_2O_3 and α-Fe_2O_3 in space group $C2/c$, see Stękiel *et al.*, 2015). In the case of $FeCrO_3$, the full $R\overline{3}c$ symmetry should be retained as long as a random distribution for cations is preferred. In contrast, if segregation of Cr^{3+} and Fe^{3+} cations in different planes parallel to {0001} is stabilized, the resulting ordered structure is isomorphous to that of ilmenite, $FeTiO_3$ (Yamanaka *et al.*, 2007), and the crystal symmetry is lowered to $R\overline{3}$ or $P\overline{3}$ if the rhombohedral Bravais lattice is retained. Finally, if cations alternate in all planes and directions, the structure is isomorphous to the low-temperature phase of $LiNbO_3$, in the space group $R3c$ (Boysen & Altorfer, 1994). To date, different laboratories are drawing contradictory conclusions, and the actual cation arrangement in $FeCrO_3$ still remains a matter of debate. The absence of superstructure peaks in X-ray (Baraton *et al.*, 1994) and, more significantly, neutron (Grygar *et al.*, 2003) powder diffraction patterns seems to be in line with a random distribution of cations. This conclusion, however, is not supported by earlier works based on vibrational spectroscopy (McCarty & Boehme, 1989; Busca *et al.*, 1993; Baraton *et al.*, 1994), giving features in agreement with an ordered, ilmenite-like structure. It is even possible to find evidence supporting *both* ordered (ilmenite) and random (corundum) cation distributions in a *single article* (Baraton *et al.*, 1994).

A direct consequence of this structural ambiguity is that the magnetic ground state of this material is not well defined. Several metastable low lying or excited states are possible, and even spin glass, spin density waves or charge density waves may be expected for the bulk. A first principles study of the crystal structure, magnetic properties and band structure of $FeCrO_3$ shows that there is little (if any) Fe—O—Cr π-type super-exchange interaction, and that the dominant coupling mechanism between Fe^{3+} and Cr^{3+} should rather be a direct ferromagnetic exchange (Moore, 2007). The magnetic ground state would thus be antiferromagnetic with a specific magnetic ordering, as in end oxides, although the bulk material could also be a spin glass. However, the most recent DFT study does not agree with this conclusion, and predicts a ferrimagnetic ilmenite-like material (Sadat Nabi & Pentcheva, 2011). The current status for $FeCrO_3$ is thus intractably obscure and controversial in many aspects. This unfortunate situation could be a consequence of the questionable quality of synthetic samples used in some studies, as claimed by some authors (*e.g.* Grygar *et al.*, 2003). Moreover, both ordered and random cation distributions might be stable, with uncontrolled variations from sample to sample. Both transition metals have similar electronegativities, and the ionic radii for Fe^{3+} (weak crystal field assumed) and Cr^{3+} in coordination 6 are almost identical, 64.5 and 61.5 pm, respectively (Shannon, 1976). Regardless of the actual structure, $FeCrO_3$ is geometrically stable, considering the tolerance factor computed on the basis of ionic radii of close-packed hard spheres (Liu *et al.*, 2009). This hypothesis of cation distribution variability is supported by simulations, which showed that segregation of Fe^{3+} and Cr^{3+} cations in $Fe_{2-x}Cr_xO_3$ is marginally favorable in energy compared with any other cation distribution (Benny *et al.*, 2009).

Our modest contribution to the complex structural issue raised by this oxide is the characterization of a naturally occurring $FeCrO_3$ crystal found in Mexico. To the best of our knowledge, no reports about this mineral were previously released. A preliminary report of our studies was presented during the SARX-2010 seminar (Reyes *et al.*, 2010).

2. Crystal analysis

We fortuitously discovered that $FeCrO_3$ is available from natural sources as large single crystals. Crystals were found in a clinoptilolite tuff known as Mexican TAM-2, extracted in the opencast mines located in Villa de Reyes (21°48' N 100°56' W), in the *Zona Centro* of San Luis Potosí State, Mexico. Felsic volcanic rocks contain most of the mineralization in this area, which belong to the *Caracol* formation, generally considered as a late Cretaceaous formation. The studied zeolitic tuff is a Si-rich clinoptilolite (Si/Al > 5), with secondary components being calcite, quartz and feldspars (Dávila-Jiménez *et al.*, 2008). Some crystals of $FeCrO_3$ may crop out at the surface of the tuff, and scanning electron microscopy–energy dispersive spectroscopy (SEM–EDS) analysis of the uncoated sample then shows the presence of both metals (Fig. 1; Jeol JSM 7800F, Oxford X-Max EDS detector). The EDS spectra extracted from these regions are comparable with those obtained on synthetic $FeCrO_3$ samples prepared by solid-state reaction between α-Fe_2O_3 and Cr_2O_3 (Ozkendir, 2013). In other regions of the material, the Cr emission lines are not detected, while Fe is always present. The

abundance of iron oxides in these samples is consistent with the underground geology and petrology of the Villa de Reyes graben (López-Loera & Tristán-González, 2013). For instance, well formed crystals of maghemite (γ-Fe_2O_3) are present in these samples, as confirmed by X-ray diffraction attempts on randomly selected crystals. Other elements detected by EDS below 5 keV originate from the clinoptilolite and associated minerals, the most abundant being Si, Al, Ca, K, Na, Mg, P, Cl and C.

The non-homogeneous nature of the native samples was confirmed by atomic absorption spectroscopy, performed on a 932 AA spectrometer (GBC Scientific) with N_2O/C_2H_2 flame atomizer and detection at λ = 357.9 nm (Cr) and λ = 248.3 nm (Fe). The sensitivity for Cr detection was 0.05 μg ml^{-1}. Samples were first treated with 5 *M* HCl, and digestion was realised in HF (1 ml, 1:10). A representative analysis carried out on a sample with a concentration of 18.675 μg ml^{-1} estimated Fe content as 0.364 μg ml^{-1} (1.94%) and Cr content as 0.185 μg ml^{-1} (0.99%). The Fe:Cr ratio of ∼ 2:1 can be interpreted as the result of a mixture of $FeCrO_3$ and iron oxides, including maghemite.

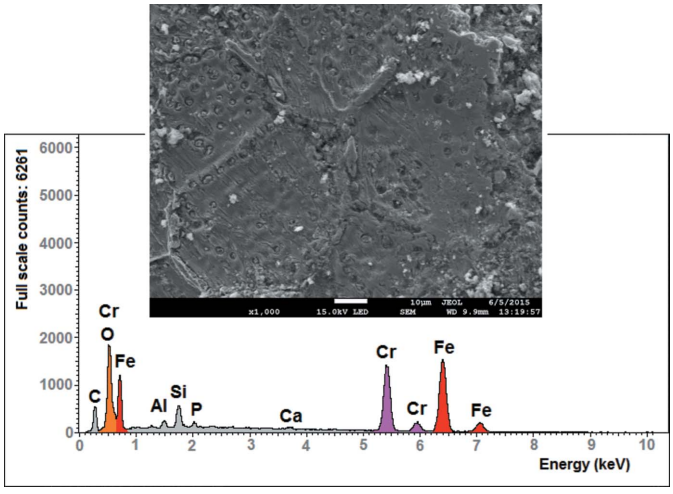

Figure 1
SEM image and EDS analysis of the tuff from which crystals of $FeCrO_3$ were obtained. The scale bar represents 10 μm. Notice the emergence of irregular hexagonal faces of embedded crystals, bounded by straight edges.

Eventually, one crystal, easily recognizable by its silver metallic luster, was separated manually from the zeolite host. The SEM image of the single crystal selected for the crystallographic and magnetic studies reported here (Fig. 2) shows a shape consistent with trigonal symmetry. X-ray diffraction data were measured at ambient temperature on a Bruker P4 diffractometer at the higher resolution of 0.58 Å in order to determine unambiguously the sites occupied by Cr (Z = 24), Fe (Z = 26) and a mixture of both metals (24 < Z < 26). Raw data were corrected for absorption effects (North *et al.*, 1968), and structural models were refined with the 2014/7 update of *SHELX* (Sheldrick, 2015). Magnetization data for the same crystal were measured in a Quantum Design magnetometer MPMS-5S.

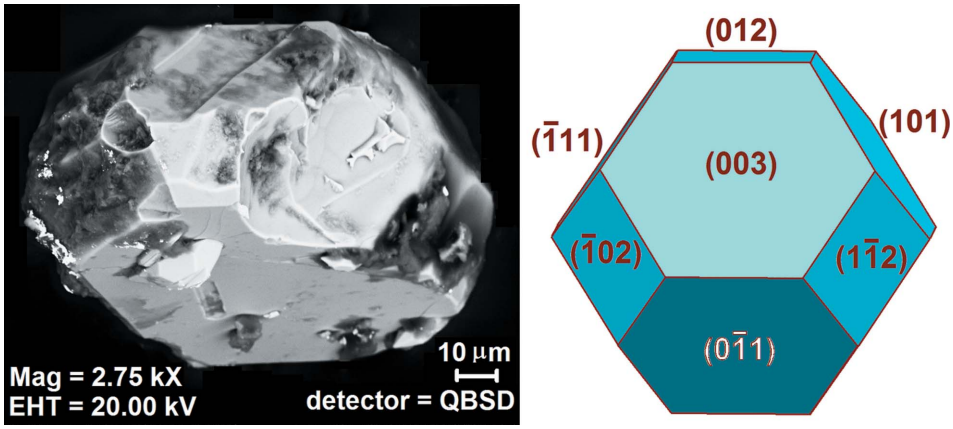

Figure 2
SEM image of the crystal used in this study, at a magnification of 2750×. The predicted crystal morphology using the BFDH model (Donnay & Harker, 1937; Macrae *et al.*, 2008) is depicted on the right side.

Table 1
Experimental details.

Crystal data	
Chemical formula	$CrFeO_3$
M_r	155.85
Crystal system, space group	Trigonal, $R\bar{3}:H$
Temperature (K)	298
a, c (Å)	5.0770 (4), 13.9621 (14)
V (Å^3)	311.67 (6)
Z	6
Radiation type	Mo $K\alpha$
μ (mm^{-1})	11.87
Crystal size (mm)	0.10 × 0.06 × 0.06
Data collection	
Diffractometer	Bruker P4
Absorption correction	ψ scan *XSCANS* (Bruker, 1997)
T_{min}, T_{max}	0.303, 0.489
No. of measured, independent and observed [$I > 2\sigma(I)$] reflections	2211, 373, 324
R_{int}	0.027
(sin $\theta/\lambda)_{max}$ (Å^{-1})	0.856
Refinement	
$R[F^2 > 2\sigma(F^2)]$, $wR(F^2)$, S	0.020, 0.059, 1.11
No. of reflections	373
No. of parameters	17
No. of restraints	0
$\Delta\rho_{max}$, $\Delta\rho_{min}$ (e Å^{-3})	0.65, −1.18

Computer programs: *XSCANS* (Bruker, 1997), *XSCANS*, *XPREP* (Bruker, 1997), *SHELXL*2014/7 (Sheldrick, 2015), *SHELXTL* (Bruker, 1997), *CaRIne Crystallography* (Boudias & Monceau, 1998).

3. Structure refinement

Crystal data, data collection and structure refinement details are summarized in Table 1. Wilson's

statistics, giving for example $\langle|E^2-1|\rangle = 1.129$ (with standard obverse hexagonal setting for the unit cell; *XPREP*, Bruker, 1997) strongly suggest a centrosymmetric space group. On the other hand, the extinction for a *c* glide plane is not present in the diffraction pattern: 89 reflections from 272 are observed at $I > 3\sigma(I)$ for the corresponding class. The crystal thus belongs to Laue class $\overline{3}$ and the space group is most likely $R\overline{3}$, as expected for an ilmenite-type structure. The starting model for refinement was ilmenite $FeTiO_3$ (Yamanaka *et al.*, 2007), with the O atom in a general position and metal atoms in special positions (0,0,z_1) and (0,0,z_2) on the threefold axis, hereafter quoted as sites [*A*] and [*B*], respectively. The structure was refined to convergence after substituting the Ti scattering factor by Cr. Fractional coordinates z_1 and z_2 converged to $z_1 = 0.14523\ (2)$ and $z_2 = 0.35412\ (2)$, with sites [*A*] and [*B*] fully occupied by Fe and Cr.

Structural models were refined mapping all stoichiometric and non-stoichiometric compositions $Fe_{2-x}Cr_xO_3$, with $0 < x < 2$ (Fig. 3). The crystallographic residual factor wR_2 based on all data was calculated for each model, as it is known to be the most sensitive to small variations in chemical composition. In these models, each [*A*] and [*B*] site was constrained to be fully occupied by a mixture of Fe and Cr. In order to avoid unstable refinements, coordinates and anisotropic displacement parameters for Fe and Cr atoms sharing the same site were constrained to be equal (*EXYZ* and *EADP* commands in *SHELXL*). Although Fe—O and Cr—O bond lengths are expected to be different, these constraints could not be relaxed, even after the introduction of a strong damping factor reducing parameter shifts between least-squares cycles. In spite of this approximation, the wR_2 factor clearly reaches a minimum for the proposed ordered structure, $[A]_{Fe}[B]_{Cr}O_3$, with $wR_2 = 0.059$. Any other $[A]_{Fe,Cr}[B]_{Cr,Fe}O_3$ distribution refines to a higher wR_2 factor. Of special interest are models matching the stoichiometric composition $FeCrO_3$ (see Fig. 3, diagonal in the map connecting $[A]_{Fe}[B]_{Cr}O_3$ to $[A]_{Cr}[B]_{Fe}O_3$). Compound $FeCrO_3$ with Fe and Cr equally distributed over [*A*] and [*B*] sites, which simulates a long-range random distribution for cations, refines to $wR_2 = 0.133$, much above the ordered model $[A]_{Fe}[B]_{Cr}O_3$. On the other hand, the ordered *anti*-distribution, $[A]_{Cr}[B]_{Fe}O_3$, refines to $wR_2 = 0.230$. For compositions approaching the *anti*-distribution, displacement parameters for [*B*] sites increase to offset the high electronic density on these sites, while displacement parameters for [*A*] sites decrease, because of the electronic deficit on these sites. These variations reflect correlations between scattering factors and displacement parameters, and support the correctness of the proposed cation distribution. These refinements also suggest that the occurrence of antisite cation defects in the crystal should be low, or at least below the limit detectable by conventional X-ray diffraction.

More difficult to estimate is the possibility of cation deficiency, because of the intrinsic correlation between site occupation factors for [*A*] and [*B*], scattering factors f_{Fe}, f_{Cr} and displacement parameters. However, an upper limit may be calculated, through a refinement with free occupancies for [*A*] and [*B*] sites. Such a refinement carried out on the ordered $[A]_{Fe}[B]_{Cr}O_3$ model affords a significant drop for wR_2, from 0.059 to 0.046, while site occupancies for Fe and Cr converge to 0.920 (5) and 0.912 (5), respectively. Roughly speaking, no more than 8% of cation sites [*A*] and [*B*] may be vacant in the crystal. Anyway, if actually present, vacancy defects are almost certainly limited to a much lower concentration, since Fe^{4+} and Cr^{4+} cations were never mentioned for $FeCrO_3$ in the literature cited in §1.

Finally, attempts to refine $FeCrO_3$ in point groups $3m1$ or $\overline{3}m1$ were unsuccessful. For example, a random distribution of cations in the space group $R\overline{3}c$ remains stuck above $wR_2 = 0.10$ and generates non-positive definite ellipsoids for metals. In the non-centrosymmetric space group $R3c$, the wR_2 factor converges to 0.12 and the Flack parameter refines inconsistently to 0.51 (3).

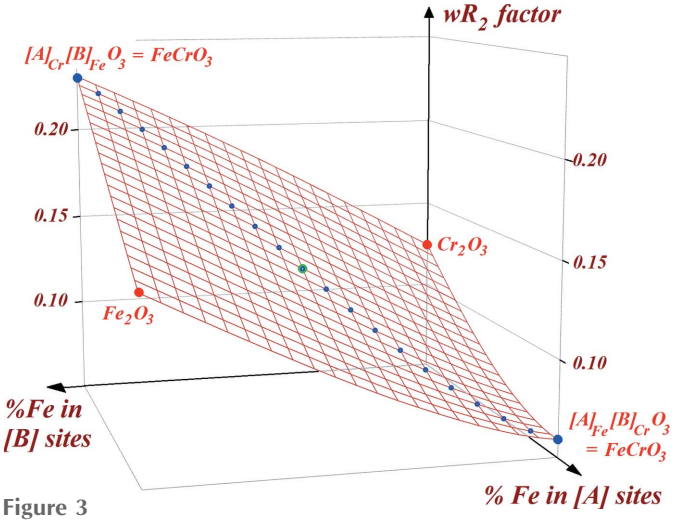

Figure 3
Refinements for $(Fe_{1-x}Cr_x)_2O_3$. A set of 441 models for $[A]_{Fe,Cr}[B]_{Fe,Cr}O_3$ compounds with [*A*] and [*B*] sites fully occupied by a mixed metal $Fe_{1-x}Cr_x$ was built: parameter *x* was varied by 0.05 steps in the range [0–1], independently for [*A*] and [*B*] sites (horizontal coordinates axis). Coordinates and displacement parameters for metals within a single site were constrained to refine to identical values, and the final wR_2 factor was calculated for each model (vertical coordinate axis). All compounds represented by a blue node have the same chemical composition, $FeCrO_3$, and the central green node is $FeCrO_3$ with a random distribution of metals in [*A*] and [*B*] sites. Two supplementary nodes correspond to stoichiometric compositions Fe_2O_3 and Cr_2O_3 (red nodes), while all the other nodes in the map are for non-stoichiometric compounds.

4. Structural commentary

In the final model (Fig. 4), [CrO_6] and [FeO_6] octahedra are trigonally distorted, the strongest deviation being observed for Cr^{3+}, with Cr—O bond lengths of 1.9003 (10) and 2.1013 (10) Å, while Fe—O distances are 2.0348 (10) and 2.1653 (10) Å. Both metal ions are thus in a C_{3v} crystal field. Since no Jahn–Teller effect is expected for a Cr^{3+} ion, such distortions should arise from packing rather than electronic effects. In spite of the largest ionic radius of Cr^{3+} compared with Ti^{4+} (Shannon, 1976), observed distortions for $FeCrO_3$ are indeed very close to those observed in $FeTiO_3$ (Yamanaka

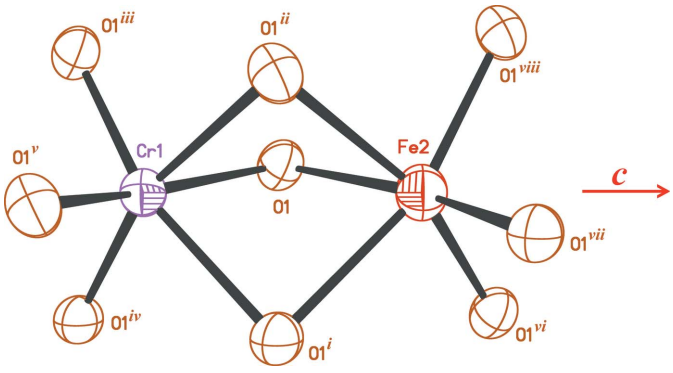

Figure 4
ORTEP-like view for face-sharing $[CrO_6]$ and $[FeO_6]$ octahedra with 99% probability level displacement ellipsoids. Atoms Cr1, O1 and Fe2 constitute the asymmetric unit, and other O atoms are generated by symmetry codes: (i) $y, x-y, z$; (ii) $-y, -x, z$; (iii) $-x+\frac{1}{3}, -y-\frac{1}{3}, -z+\frac{2}{3}$; (iv) $y+\frac{1}{3}, -x+y+\frac{2}{3}, -z+\frac{2}{3}$; (v) $-x+y+\frac{2}{3}, x-\frac{1}{3}, -z+\frac{2}{3}$; (vi) $-x+\frac{2}{3}, -y+\frac{1}{3}, -z+\frac{1}{3}$; (vii) $-y-\frac{1}{3}, -x+y+\frac{1}{3}, -z+\frac{1}{3}$; (viii) $x-y-\frac{1}{3}, x-\frac{2}{3}, -z+\frac{1}{3}$.

et al., 2007). In the crystal, Fe^{3+} and Cr^{3+} ions are segregated in layers formed by $[CrO_6]$ and $[FeO_6]$ octahedra, and layers alternate along the trigonal *c*-axis (Fig. 5). For two neighboring $[CrO_6]$ edge-sharing octahedra, equatorial mean planes are coplanar by symmetry, and the mean deviation of O^{2-} ions from this plane is 0.076 Å. The Cr^{3+} ion is shifted by 0.202 Å out of this equatorial plane. Regarding $[FeO_6]$ octahedra, a similar arrangement is observed, but the mean deviation for O^{2-} ions from the equatorial plane is limited to 0.002 Å, with the metal placed 0.226 Å out of the plane. An important structural feature related to the magnetic properties of $FeCrO_3$ is the Cr—O—Fe angle of 134.33 (5)° between vertex-sharing octahedra in two neighboring layers (see top–left inset in Fig. 5), since it has been related to a super-exchange interaction along Fe—O—Cr (Lenglet *et al.*, 1995). In the solid, the shortest interlayer Fe···Cr metal–metal separation is 2.9166 (6) Å, whereas non-bonding Cr···Cr and Fe···Fe separations within layers are slightly longer, 2.9881 (3) and 2.9917 (3) Å, respectively.

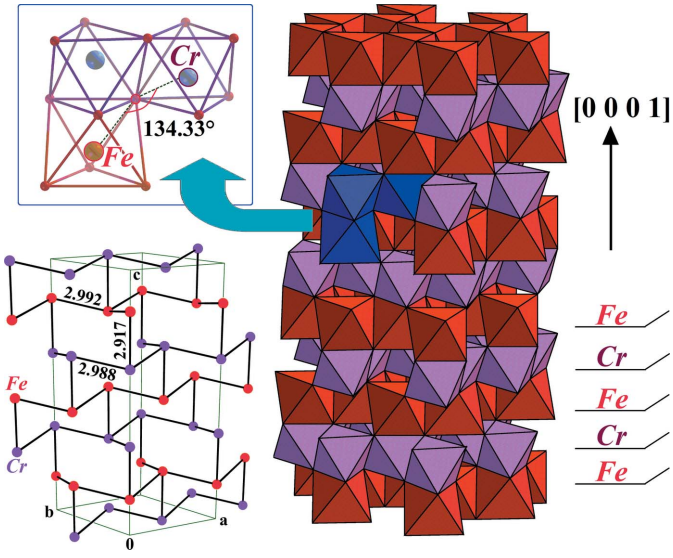

Figure 5
Single crystal structure of $FeCrO_3$ using the polyhedral representation (Boudias & Monceau, 1998), showing the packing of Fe and Cr layers along the *c* axis. Three octahedra, represented in blue in the main figure, are displayed in the top–left inset. Two $[CrO_6]$ octahedra belonging to the same layer share one edge, while $[CrO_6]$ and $[FeO_6]$ octahedra in two neighboring layers are sharing one face. The Cr—O—Fe angle of 134.33 (5)° involved in magnetic interactions is shown. The bottom–left figure shows the shortest metal···metal distances in the crystal, in Å. O atoms have been omitted for clarity.

Magnetization *versus* applied field studies were carried out in a squid magnetometer in the 2–325 K temperature range. A hysteresis behavior is clearly observed over the whole temperature range (Fig. 6). Maximum and minimum magnetization extracted from $M(T)$ curves obtained at $H = 1$ T are 0.155 emu at 2 K and extrapolated to 0.053 emu at 1050 K. Such an inverse dependence of M *versus* T is close to a Brillouin-type behavior (Morrish, 2001), in agreement with a ferromagnetic or ferrimagnetic ordering at all temperatures between 2 K and 1050 K.

The Cr—O—Fe angle of 134.33 (5)° and the $Fe^{3+}\cdots Fe^{3+}$ separation of 2.9917 (3) Å within Fe layers (see Fig. 5) can produce the antiferromagnetic interaction between Fe^{3+} and Cr^{3+} ions (Lenglet *et al.*, 1995). The two antiferromagnetic phases then alternate along the *c* axis, one soft Cr_2O_3 layer with Néel temperature $T_N = 307$ K, and the other one being magnetically hard, Fe_2O_3, with Néel temperature $T_N = 955$ K. We assume that both magnetic phases form canted spin populations, and that uncompensated canted magnetic moments occur between the soft and hard magnetic phases. The upper bound limit for the thickness of the interface involved in exchange interactions may be estimated from the size of O^{2-} ions, considered as 2.8 Å diameter hard spheres

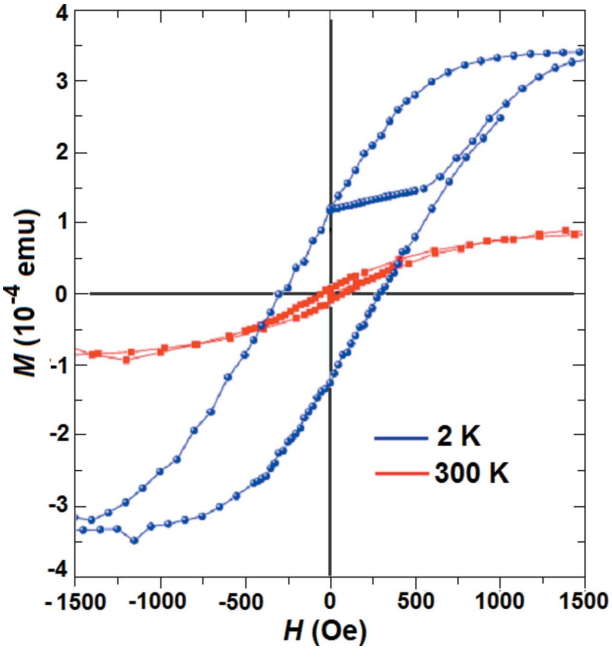

Figure 6
Isothermal hysteresis loops $M = f(H)$ at 2 K (blue dots) and 300 K (red dots), showing the coercive fields and remanent magnetization for the $FeCrO_3$ single crystal of Fig. 2.

(Shannon, 1976). This magnetic description, based on the ordered crystal structure, is in agreement with first principles studies of magnetic coupling in $(Fe_xCr_{1-x})_2O_3$ reported by Seyed Hasan Sadat Nabi in his thesis (Sadat Nabi, 2010; Sadat Nabi & Pentcheva, 2011).

As mentioned in §1, the possible existence of non-ordered $FeCrO_3$ phases should not be ruled out, which could have different spectroscopic and magnetic properties in comparison to the mineral characterized here. Caution should be exercised, for example, when assessing the reliability of unit-cell parameters of these crystalline materials. In the present study, the axial ratio c/a = 2.75 obtained for the trigonal cell (see Table 1) deviates significantly from DFT calculations using B3LYP functional, c/a = 2.72 or 2.73 (Moore, 2007). This calculated figure has indeed been observed experimentally for crystalline samples obtained from oxides (c/a = 2.73; Loudghiri *et al.*, 2000), nanocrystalline gels (c/a = 2.72; Bhattacharya *et al.*, 1997), gel samples (c/a = 2.72; Grygar *et al.*, 2003), and fine powders obtained by coprecipitation (c/a = 2.73; Baraton *et al.*, 1994). However, as suggested by some authors, these *synthetic* materials could be metastable, due to miscibility problems avoiding the fast crystallization of an ordered structure. Regarding the titanium-based ilmenite $FeTiO_3$, the observed axial ratio, c/a = 2.77, is higher (Yamanaka *et al.*, 2007), as expected: if Fajan's rules hold, the hard cations Ti^{4+} polarize the Ti—O bonds, increasing the covalent character for the Ti-based ilmenite.

Furthermore, the average structure depicted by X-ray diffraction is not adequate to identify whether the crystal is affected by short-range microtwinning. In particular, the stacking fault for Cr and Fe layers could make the ordered structure prone to polytypism, and even generate allotwins.

5. Conclusions

The discovery of naturally occurring $FeCrO_3$ samples suitable for single-crystal X-ray characterization and magnetic studies was fortunate, since so far no straight and reproducible synthesis for the bulk material has been established. In this new mineral, Fe^{3+} and Cr^{3+} ions are ordered in alternating layers, allowing hard and soft magnetic phases to stack along the crystallographic threefold axis of the material. It is worth noting that the threefold symmetry is indeed an inheritance from parent oxides, which both display the corundum structure. We thus assume that crystallization of the ordered mineral should be limited by very slow kinetics, which should require geological times to be efficiently equilibrated. This makes a difference with samples obtained through solid-state synthesis techniques, for which fast kinetics may induce a frustrated order, and could explain discrepancies between pictures provided by spectroscopic techniques and powder X-ray diffraction in the early literature.

This account is very reminiscent of the 'lamellar magnetism' concept developed 10 years ago by the group of Rob Hargraves at Princeton University (Robinson *et al.*, 2002, 2004). This group successfully modeled ilmenite lamella at the short-range scale in a canted antiferromagnetic hematite host, to explain the 'chemical' remanent ferrimagnetism of exsolved members of the hematite–ilmenite solid-solution series. These materials are present in some slowly cooled igneous and metamorphic rocks, which are known to display unusually strong and stable remanent magnetization, and we believe that ferrimagnetic $FeCrO_3$ belongs to this class of oxides. On the other hand, the controlled synthesis of this oxide containing coherently intergrown phases should be considered, at the very least, as a challenging task (McEnroe *et al.*, 2007). The challenge would be to emulate the cation ordering process through an extremely slow temperature decrease, whilst avoiding exsolution of the parent oxides below the temperature of stability of the ilmenite-like solid solution.

Acknowledgements

We are indebted to J. R. Ramos Durán (Comercializadora Zeolite, SLP, Mexico) for kindly providing rocks of zeolitic tuff, and Omar Novelo Peralta (UNAM) for preliminary SEM studies. MAPC acknowledges grant 153848 from CONACyT (Mexico). RE gratefully acknowledges partial support from CONACyT (project 129203, Ciencia Básica), DGAPA-UNAM (project No. IN106014), EU-Mexico BisNano Scientific Collaboration, and The Institute of Sciences and Technology of Distrito Federal, Mexico (ICyT, project PICCO 11-7 and grant for new infrastructure). SB thanks ICUAP for diffractometer time. RSG acknowledges partial support from CONACyT (Project 163153). We also acknowledge useful comments by referees of a previous submission to another journal, and the interesting feedback provided by the referees of the manuscript submitted to *Acta Cryst.*

References

Baca Arroyo, R., Galván Arellano, M., Peña Sierra, R. & Andraca Adame, J. A. (2012). 2nd International Conference on Materials, Mechatronics and Automation (ICMMA 2012), *Lecture Notes in Information Technology*, Vol. 15, pp. 146–151.

Baraton, M. I., Busca, G., Prieto, M. C., Ricchiardi, G. & Escribano, V. S. (1994). *J. Solid State Chem.* **112**, 9–14.

Benny, S., Grau-Crespo, R. & de Leeuw, N. H. (2009). *Phys. Chem. Chem. Phys.* **11**, 808–815.

Bhattacharya, A. K., Hartridge, A., Mallick, K. K., Majumdar, C. K., Das, D. & Chintalapudi, S. N. (1997). *J. Mater. Sci.* **32**, 557–560.

Boudias, A. & Monceau, D. (1998). *CaRIne Crystallography*, Version 3.1. Software CaRIne Crystallography, Senlis, France.

Boysen, H. & Altorfer, F. (1994). *Acta Cryst.* B**50**, 405–414.

Bruker (1997). *XSCANS, XPREP* and *SHELXTL*. Bruker AXS Inc., Madison, Wisconsin, USA.

Busca, G., Ramis, G., Prieto, M. del C. & Escribano, V. S. (1993). *J. Mater. Chem.* **3**, 665–673.

Dávila-Jiménez, M. M., Elizalde-González, M. P., Mattusch, J., Morgenstern, P., Pérez-Cruz, M. A., Reyes-Ortega, Y., Wennrich, R. & Yee-Madeira, H. (2008). *J. Colloid Interface Sci.* **322**, 527–536.

Donnay, J. D. H. & Harker, D. (1937). *Am. Mineral.* **22**, 446–467.

Grygar, T. (1999). *J. Electrochem. Soc.* **146**, 3234–3237.

Grygar, T., Bezdička, P., Dědeček, J., Petrovský, E. & Schneeweiss, O. (2003). *Ceram. Silik.* **47**, 32–39.

Klinger, R., Ensling, J., Jachow, H., Meisel, W., Schwab, E. & Gütlich, P. (1995). *J. Magn. Magn. Mater.* **150**, 277–283.

Lenglet, M., Hochu, F. & Musić, S. (1995). *Solid State Commun.* **94**, 211–215.

Liu, X. C., Hong, R. & Tian, C. (2009). *J. Mater. Sci. Mater. Electron.* **20**, 323–327.
López-Loera, H. & Tristán-González, M. (2013). *Bol. Soc. Geol. Mexicana*, **65**, 137–156 (in Spanish).
Loudghiri, E., Belayachi, A., Nogues, M., Taibi, M., Dahmani, A., Yamani, M. E. & Aride, J. (2000). *M. J. Condens. Matter.* **3**, 98–105.
Macrae, C. F., Bruno, I. J., Chisholm, J. A., Edgington, P. R., McCabe, P., Pidcock, E., Rodriguez-Monge, L., Taylor, R., van de Streek, J. & Wood, P. A. (2008). *J. Appl. Cryst.* **41**, 466–470.
McCarty, K. F. & Boehme, D. R. (1989). *J. Solid State Chem.* **79**, 19–27.
McEnroe, S. A., Carter-Stiglitz, B., Harrison, R. J., Robinson, P., Fabian, K. & McCammon, C. (2007). *Nature Nanotech.* **2**, 631–634.
Moore, E. A. (2007). *Phys. Rev. B*, **76**, 195107.
Morrish, A. H. (2001). *The Physical Principles of Magnetism*, edited by R. J. Herrick, pp. 332–416. New York: the Institute of Electrical and Electronics Engineers.
Murakami, Y., Sawata, A. & Tsuru, Y. (1999). *J. Mater. Sci.* **34**, 951–955.
Murakami, Y., Sawata, A., Tsuru, Y. & Akiyama, K. (2003). *J. Mater. Sci.* **38**, 2723–2725.
Musić, S., Lenglet, M., Popović, S., Hannoyer, B., Czakó-Nagy, I., Ristić, M., Balzar, D. & Gashi, F. (1996). *J. Mater. Sci.* **31**, 4067–4076.
Musić, S., Popović, S. & Ristić, M. (1993). *J. Mater. Sci.* **28**, 632–638.
North, A. C. T., Phillips, D. C. & Mathews, F. S. (1968). *Acta Cryst.* A**24**, 351–359.
Ozkendir, O. M. (2013). *J. Electron Spectrosc. Relat. Phenom.* **191**, 54–59.
Reyes, Y., Pérez, M. A., Elizalde, M. P., Escudero, R., Bernès, S. & Zamorano, R. (2010). *XII Latin American Seminar of Analysis by X-ray Techniques* (SARX-2010).
Robinson, P., Harrison, R. J., McEnroe, S. A. & Hargraves, R. B. (2002). *Nature*, **418**, 517–520.
Robinson, P., Harrison, R. J., McEnroe, S. A. & Hargraves, R. B. (2004). *Am. Mineral.* **89**, 725–747.
Sadat Nabi, S. H. (2010). PhD thesis, Ludwig-Maximilians University, Munich, Germany.
Sadat Nabi, H. & Pentcheva, R. (2011). *Phys. Rev. B*, **83**, 214424.
Schmuki, P. (1998). *J. Electrochem. Soc.* **145**, 791–801.
Shannon, R. D. (1976). *Acta Cryst.* A**32**, 751–767.
Sheldrick, G. M. (2015). *Acta Cryst.* C**71**, 3–8.
Stękiel, M., Przeniosło, R., Sosnowska, I., Fitch, A., Jasiński, J. B., Lussier, J. A. & Bieringer, M. (2015). *Acta Cryst.* B**71**, 203–208.
Tsokov, P., Blaskov, V., Klissurski, D. & Tsolovski, I. (1993). *J. Mater. Sci.* **28**, 184–188.
Vayssieres, L., Guo, J. & Nordgren, J. (2001). *J. Nanosci. Nanotechnol.* **1**, 385–388.
Yamanaka, T., Komatsu, Y. & Nomori, H. (2007). *Phys. Chem. Miner.* **34**, 307–318.